April 16, 2002
OPERA Note #30

RESULTS ABOUT H7546 MULTIANODE PMT's STUDIES

R. Arnold, E. Baussan, M. Dracos, B. Dorion,
J–P. Engel, J–L. Guyonnet, J. Cailleret,
G. Gaudiot, B. Humbert, R. Igersheim, T–D. Le,
D. Staub, D. Thomas, J. Wurtz

IReS, IN2P3–CNRS/Université Louis Pasteur
BP 28, F-67037 Strasbourg Cedex 2, France.

Abstract

In this report, results about characteristics of the Hamamatsu multianode photomultipliers which have been chosen to equip the Target Tracker of OPERA experiment are presented. The gain variation with supplied voltage and the crosstalk between adjacent channels have been carefully studied for 4 tubes.

1. Introduction

This document is organized in three parts. The first part briefly summarizes the model used in the analysis describing physical processes occurring in the dynode chain. Then, the characteristics of the experimental test setup CHARLY and the mechanical procedure for PMT's alignment are presented .
The final part deals with measurements and results about gain and crosstalk.

2. Spectral analysis.

The model of the photomultiplier response function used in this analysis is based on the deconvolution of the charge spectrum as presented in [1]. It was used for the analysis of photomultipliers with one system of dynodes. However, it can be applied for the Hamamatsu multianode PMT's.
In the first part, the main features of the H7546 multianode PMT are described and in the last two parts the main physical processes are summarized in order to explain the shape of the signal and the detailed function used for the analysis.

2.1. PMT description.

The H7546 Hamamatsu PMT has 64 independent channels. Each channel covers a surface of 2.3 $\times$ 2.3 mm^2 and has two series of 12 dynodes. A double grid of focalization electrodes (Fig. 1) separates the PMT channels while a single electrode separates the two dynode openings of the same channel. An output from each channel is provided.

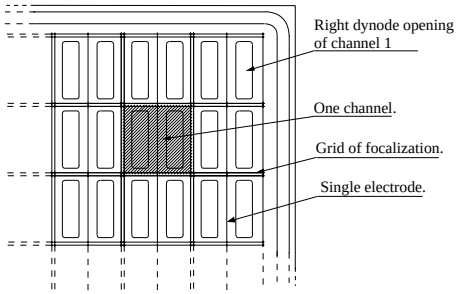

Figure 1. Partiel view (window side) of the H7546 Hamamatsu PMT.

2.2. Physical processes.

Two statistical processes mainly occur in a PMT and can be considered independently. The first one is photoconversion on the photocathode.

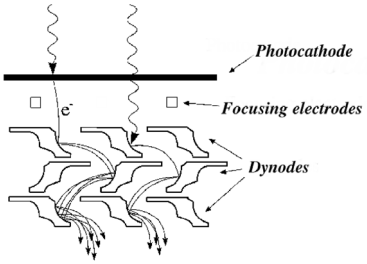

Figure 2. Schematic view of dynode chain amplification.

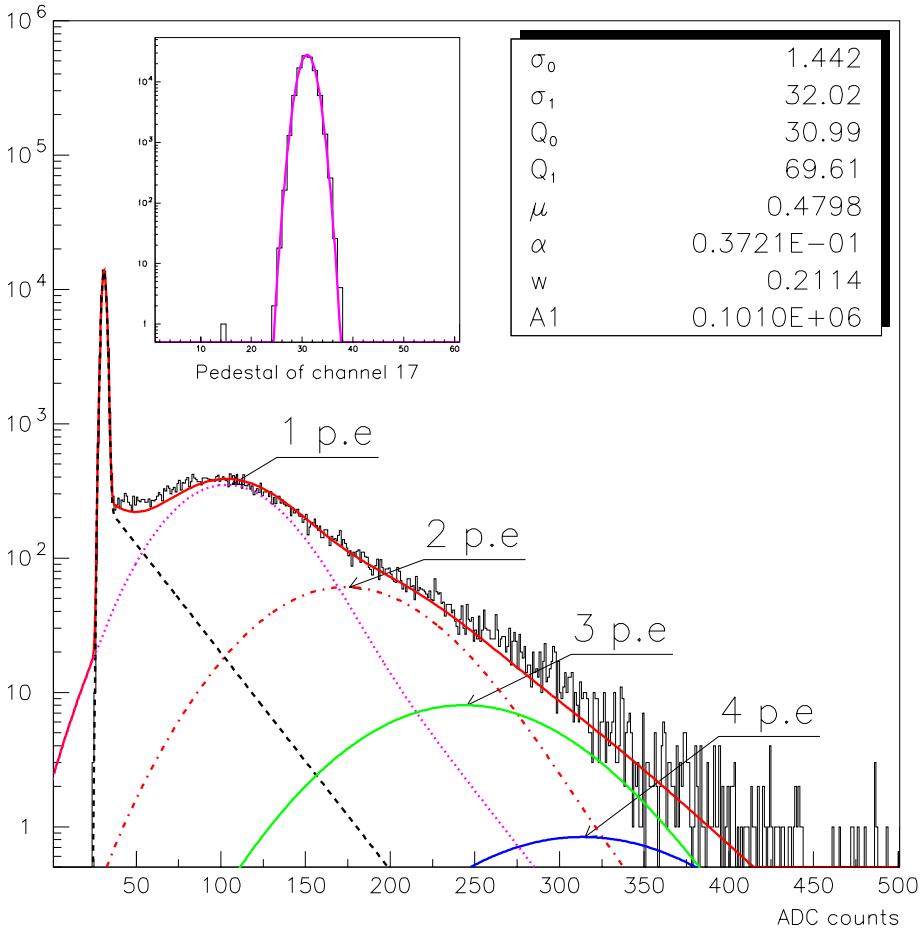

Figure 3. Example of charge spectrum obtained on channel #17 of the PMT GA0229 at 850 V. The fiber was located at the center of the channel.

The distribution of emitted photoelectrons follows a Poissonian distribution $P_\mu(n)$:

$$P_\mu(n) = \frac{\mu^n}{n!}e^{-\mu} \quad \text{with} \quad \mu =< n_{pe} >=< n_\gamma > .\varepsilon_q.\eta_c,$$

where $< n_\gamma >$ is the mean number of photons hitting the photocathode, ε_q its quantum efficiency and η_c the collection efficiency on the first dynode.

The second process is the amplification by the 12 dynodes (Fig. 2). The signal is described by a Gaussian distribution $G_{Q,\sigma}$ of mean charge Q and standard deviation σ as the result of a sum of a Poissonian emission for each dynode. Q is related to the n photoelectron charge $Q_{pe} = n.e$ (where e is the charge of the electron) through the gain G :

$$Q = G.Q_{pe}$$

So the response for a PMT with one chain of dynodes (named d_1) is a convolution between the two distributions [2]:

$$S_{d_1}(q) = [P_\mu \otimes G_{Q,\sigma}](q)$$

However, in the case of the H7546 multianode PMT, there are two parallel systems of dynodes for each anode. Consequently, a single photoelectron passes through one of the two dynode systems inducing on the

anode a charge Q_1 or Q_2. The ideal signal of the channel is given by :

$$S_{ideal}(q) = [P_\mu \otimes \mathcal{R}_{Q_1,\sigma_1,Q_2,\sigma_2}](q)$$

where $\mathcal{R}_{Q_1,\sigma_1,Q_2,\sigma_2}(q)$ is the one photoelectron response of the two dynode chain. Two reasonable hypothesis allow to make an approximation of the response distribution, the gain difference between the two chains is weak, and the photoelectron repartition is supposed symmetric when the photons strike the photocathode in the center of the channel. In this case, the response distribution can be approximated by a Gaussian:

$$\begin{aligned}\mathcal{R}_{Q_1,\sigma_1,Q_2,\sigma_2}(q) &= \tfrac{1}{2}\big[G(Q_1,\sigma_1) + G(Q_2,\sigma_2)\big] \\ &\simeq G_{<Q>,<\sigma>},\end{aligned}$$

where $< Q >= \frac{Q_1+Q_2}{2}$ and $< \sigma >^2 \simeq \frac{\sigma_1^2+\sigma_2^2}{2}$.

Consequently,

$$S_{ideal}(q) \simeq [P_\mu \otimes G_{<Q>,<\sigma>}](q).$$

The formule used to describe one dynode chain can be used.

2.3. The analysis function.

On the signal described in the previous section, a noise component must be added. The pedestal is represented by a Gaussian function $G_{Q_0,\sigma_0}(q)$. The photoelectric effect on first dynode approximated by an exponential function with a characteristic charge $Q_\alpha = \frac{1}{\alpha}$ has to be taken into account. If w is the "weight" of this signal, the total extra contribution due to noise and photoconversion on the first dynode is evaluated to be the barycentre of the two processes :

$$\begin{aligned}B_{\alpha,w,Q_0,\sigma_0}(q) &= (1-w).\tfrac{1}{\sqrt{2\pi}\sigma_0} e^{-\frac{(q-Q_0)^2}{2\sigma_0^2}} \\ &\quad + w.\theta(q-Q_0).\alpha.e^{-\alpha(q-Q_0)},\end{aligned}$$

where $\theta(q - Q_0)$ is the Heaviside function. The mean value of the charge is then shifted by the mean value of this second component:

$$\begin{aligned}< Q >_{extra} &= \int q.B_{\alpha,w,Q_0,\sigma_0}(q) \\ &= Q_0 + w.Q_\alpha.\end{aligned}$$

The realistic signal distribution, involving 7 parameters, is a convolution between this extra signal and the ideal parameters :

$$S_{Q_0,\sigma_0,Q,\sigma,\alpha,w,\mu}(q) = [S_{ideal_{Q,\sigma,\mu}} \otimes B_{\alpha,w,Q_0,\sigma_0}](q)\ .$$

Developing this expression, the result gives the analysis function $S_{fit}(q)$:

$$\begin{aligned}&S_{fit}(q) = \\ &\sum_{n=0} \frac{\mu^n e^{-\mu}}{n!}\Bigg\{(1-w)\frac{1}{\sqrt{2\pi}\sigma_n} e^{-\frac{(q-Q_n)^2}{2\sigma_n^2}} \\ &+w.\frac{\alpha}{2} e^{-\alpha(q-Q_n-\alpha.\sigma_n^2)} \\ &.\Bigg[erf\left(\frac{|Q_0-Q_n-\alpha.\sigma_n^2|}{\sigma_n\sqrt{2}}\right) + sign(q-Q_n-\alpha.\sigma_n^2) \\ &.erf\left(\frac{|q-Q_n-\alpha.\sigma_n^2|}{\sigma_n\sqrt{2}}\right)\Bigg]\Bigg\},\end{aligned}$$

with :

$$\begin{aligned}Q_n &= Q_0 + nQ \\ \sigma_n &= \sqrt{\sigma_0^2 + n\sigma^2}.\end{aligned}$$

The Poisson term gives the occurrence probability of the n photoelectron signal. In the analysis, pedestal characteristics are independently fixed by a Gaussian fit, using special pedestal runs. The other parameters are determined fitting the complete formula. An example of a global fit is shown Fig. 3. The fit is performed using a likelihood method within the MINUIT package [3].

3. Experimental setup.

In this part, the experimental chain used for testing multianode PMT's is described as well as the mechanical alignment procedure.

3.1. The experimental setup CHARLY.

The setup was originally developed for testing the 2000 photomultipliers of NEMO double-β experiment [4] and updated for the multianode PMT's [5].

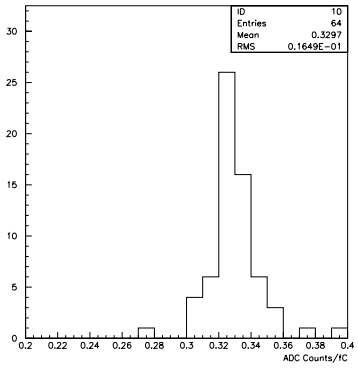

Figure 4. Distribution of the electronic gain slopes for the 64 amplifiers.

It consists of a X-Y table which allows 12.5 μm steps in both directions. In order to reproduce the equivalent light expected in the OPERA Target Tracker [6], a WLS fiber of 1 mm diameter separated in two parts is used to illuminate the photocathode. Inserted in a PMMA depolished cylinder, this fiber collects and transmits the light (mean wave length 470 nm) emitted by a pulsed LED at 300 Hz. The intensity is regulated varying the distance between the two parts (one in front of the other) of the fiber, allowing a fine tuning around the single photoelectron level. In order to monitor the stability of the light source, a reference PMT is added in the PMMA cylinder. The optical contact between the fiber and the H7546 photocathode is realized by Bicron optical grease BC-630.
PMT's are fixed on the test setup by the intermediate of a plastic collar (Fig. 6) of which fixations are determined by a mechanical procedure explained in the next section. The system assures the same positioning for each PMT scanning. All signals are shaped by a 64 amplifier box built by Bern University. Calibration curves were established by injecting a pulsed signal on a 1 pF capacitor. The distribution of the slopes is shown Fig. 4.

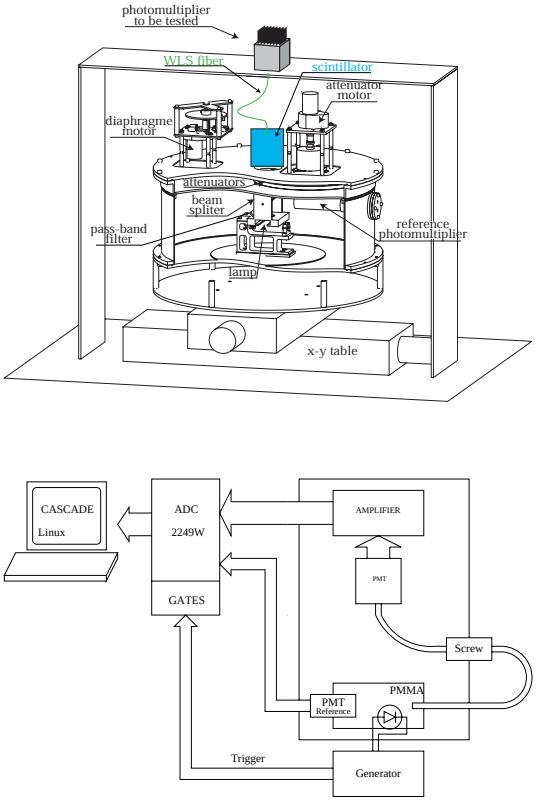

Figure 5. Sketch of the PMT setup.

All the 64 channels are connected to LeCroy 2249W ADC's read out by a Linux station. The acquisition system is controlled by CASCADE [7] (Fig. 5).

3.2. Mechanical alignment of PMT's.

For each scanning, the same positioning for all the 64 channels is required. A mechanical method proposed by Bern Universtity has been established using two plastic pieces.

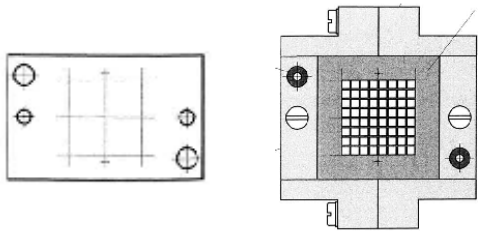

Figure 6. Plexiglass grid (left) and collar+PMT set necessary for alignment (right) .

Each PMT is tightened in a plastic collar to form a set (Fig. 6 right). The aim of the alignment procedure is to precisely determine the position of this set in order to provide the same geometrical position of channels for each scanning.

A reference system common to the PMT system and the x-y scanning setup has to be defined. One of them is fixed (arm) and the other is determined by the PMT's geometrical characteristics. Each system has two references which are aligned with the help of two guiding pins.
In order to determine the precise location where to drill the two holes on the PMT set, a second transparent plexiglass piece is used (Fig. 6 left) on which is represented :

- a square contour with its medians which has the dimension of the surface of the 64 channels (18.1x18.1 mm^2),
- two holes which will help to drill the reference holes on the PMT.

The aim of the manipulation is to align the medians with the focalization electrodes inside the PMT [8] under a binocular by positionning the plexiglass piece on the photocathode.

4. Measurements.

Each PMT provides 64 signals coming from the channels and an extra signal called *Dynode 12 signal* (Dy12) which represents the total charge over all the 64

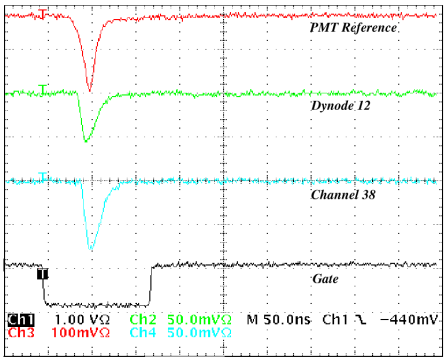

Figure 7. Example of typical signals at single photoelectron level for the PMT GA0229 (850 V).

channels.

The light can be controlled by the supplied voltage of the LED and, more precisely, by the screw acting on the distance between the 2 parts of the fiber.
When the fiber is placed in front of a channel, the light intensity is measured by this channel and Dy12. A typical signal at single photoelectron level is represented Fig. 7.

4.1. Preliminary measurements.

The first stage of the analysis consists in the scanning of the photocathode with the 1 mm WLS fiber.
The size of measurement steps is 0.25 mm (= 20 CHARLY steps) in X and Y directions. A full scan of 100×100 measurement points on all the surface takes about 24 hours. An example of charge distribution $Q_i(x, y)$ of each channel i and the sum over the 64 channels is shown Fig. 8 :

$$Q(x, y) = \sum_{i=1}^{64} Q_i(x, y)$$

4.2. Channels localization procedure.

The main problem for this analysis is to localize the geometrical center of all channels. However, the precise analysis of a channel reveals a variation on the number of collected photoelectrons versus the fiber position of the order of 6% (Fig. 9a,b). The observed loss when the WLS fiber is at the center of the channel is due to a photoelectron collection by the focalization electrode separating the two dynode systems. Thus, the maximum gain and charge is not located at the geometrical center but when the WLS fiber is in front of one of the two

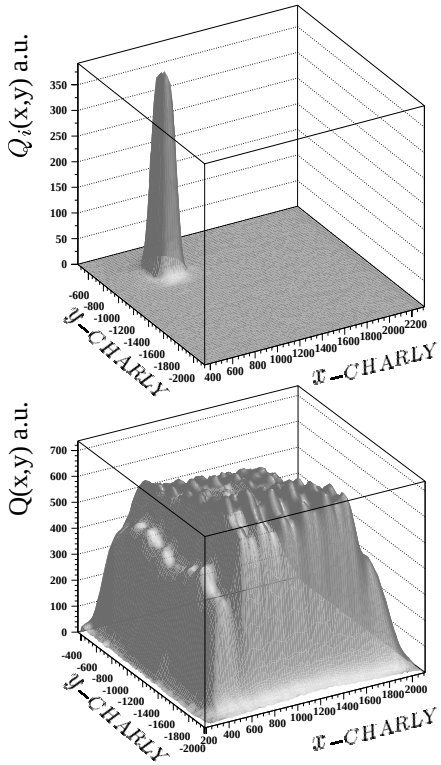

Figure 8. Charge distribution of channel #10 and sum of the 64 collected charges for PMT GA0036 at 850 V (1 scanning step = 20 CHARLY steps = 0.25 mm).

dynodes, as presented by Fig. 9c.

In order to localize the center of each channel, a virtual grid composed by 64 points corresponding to the center of the channels is adjusted over the total charge distribution. It has 3 parameters : X_G, Y_G which represents the center of the grid and θ_G a rotation angle between the channel direction and the CHARLY displacement. So, the (X_i, Y_i) coordinates of a channel i, can be expressed with the help of these parameters :

$$\begin{bmatrix} X_i \\ Y_i \end{bmatrix} = \begin{bmatrix} cos(\theta_G) & sin(\theta_G) \\ -sin(\theta_G) & cos(\theta_G) \end{bmatrix} \begin{bmatrix} X_G + n_i.\Delta X \\ Y_G + m_i.\Delta Y \end{bmatrix}$$

where ΔX, ΔY correspond to the width of a channel (2.3 mm), n_i and m_i are the row and column numbers of channel i.
As the maximum charge collected in a channel is located on one of the two dynodes, the values of parameters X_G, Y_G, θ_G evaluated by maximizing the sum of all charges would be biased and cannot be used to find the center of each channel.
A charge $\mathcal{Q}_i$ defined by integrating the following quantity on a small surface $\delta_x \delta_y$ centered on channel i and covering both dynode openings is considered :

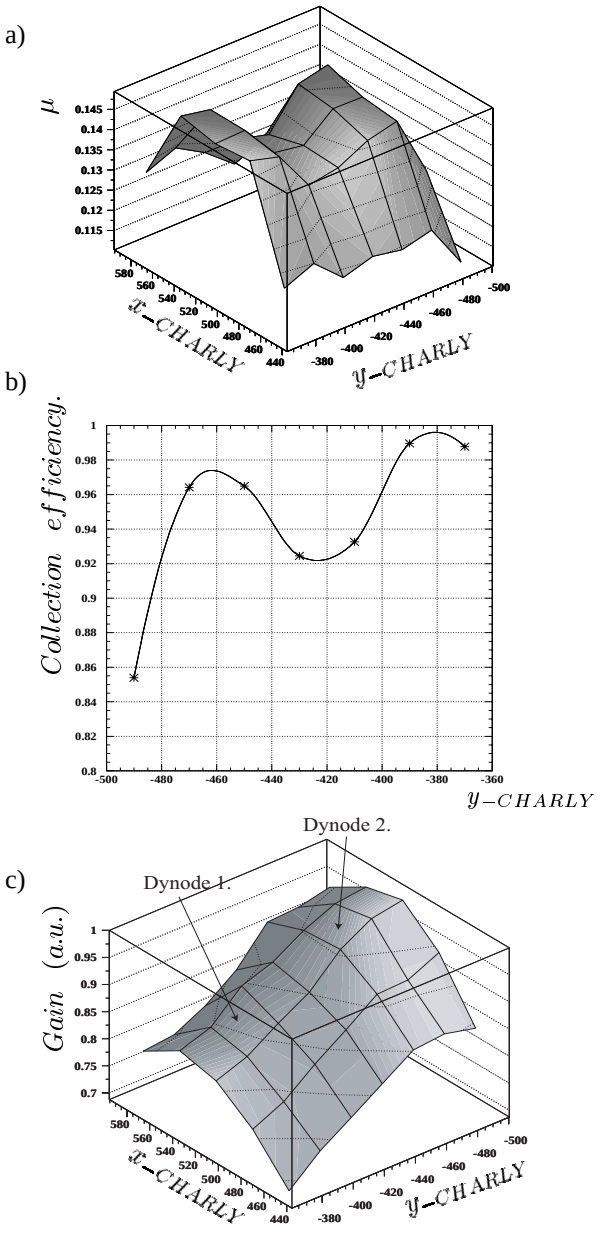

Figure 9. Fine scanning of channel #10 for the PMT GA0036 (850 V).

a) Mean number of photoelectrons versus position.
b) Normalized mean number of photoelectrons in median plane x=516.
c) Gain versus position.

$$\mathcal{Q}_i(X_G, Y_G, \theta_G) = \int_{X_i - \frac{\delta_x}{2}}^{X_i + \frac{\delta_x}{2}} \int_{Y_i - \frac{\delta_y}{2}}^{Y_i + \frac{\delta_y}{2}} Q_i(x,y)dxdy,$$

where $Q_i(x,y)$ is the charge distribution of channel i. Maximizing this charge by fitting X_G, Y_G and θ_G would give better results. The parameters δ_x and δ_y must not be defined too small to avoid the bias previously described. To increase the channel location accuracy, another quantity using the optical crosstalk on neighbouring channels was defined. This crosstalk must be minimal and symmetric over the neighbouring channels. The charge of channel i when the fiber is located in x,y position is given by $Q_i(x,y)$. Consequently, the total crosstalk will be calculated by integrating all the individual charge distributions $Q_j(x,y)$ of its neighbours j around the (X_i, Y_i) position:

$$\mathcal{Q}_i^c(X_G, Y_G, \theta_G) =$$

$$\sum_{j=1}^{Neighbours\ of\ i} \int_{X_i - \frac{\delta_x}{2}}^{X_i + \frac{\delta_x}{2}} \int_{Y_i - \frac{\delta_y}{2}}^{Y_i + \frac{\delta_y}{2}} Q_j(x,y)dxdy,$$

where $\mathcal{Q}_i^c(X_G, Y_G, \theta_G)$, represents the total charge collected by the neighbours of channel i.
The correct parameter values are given by maximizing the charge and minimizing this crosstalk. The ratio of this two quantities has to be maximized for all the channels :

$$R_{PMT}(X_G, Y_G, \theta_G) = \sum_{i=1}^{64} \frac{\mathcal{Q}_i(X_G, Y_G, \theta_G)}{\mathcal{Q}_i^c(X_G, Y_G, \theta_G)}.$$

These 3 parameters define the 64 positions of the PMT channels for the following analysis.
After finding the center of each channel, three measurements are realized for each channel to study the gain uniformity at the geometrical center, defined previously, and at the position of each dynode (separated by $\pm$ 0.5 mm by construction). The intensity of light is reduced around the single photoelectron level.

4.3. Gain distribution.

The gain evaluated in the center of the channels is given by the mean value of gains of the two dynode systems.
The gain is an important intrinsic feature of the dynode chains and was measured for all the 64 channels. The results are shown Fig. 12, 13, 14, 15, for the same supplied voltage 850 V for 4 different PMT's.
The mean gain evaluated in the central channel positions is defined by :

$$< G(V) >^{central} = \frac{1}{N} \sum_{i=1}^{N} G_i^{central}(V).$$

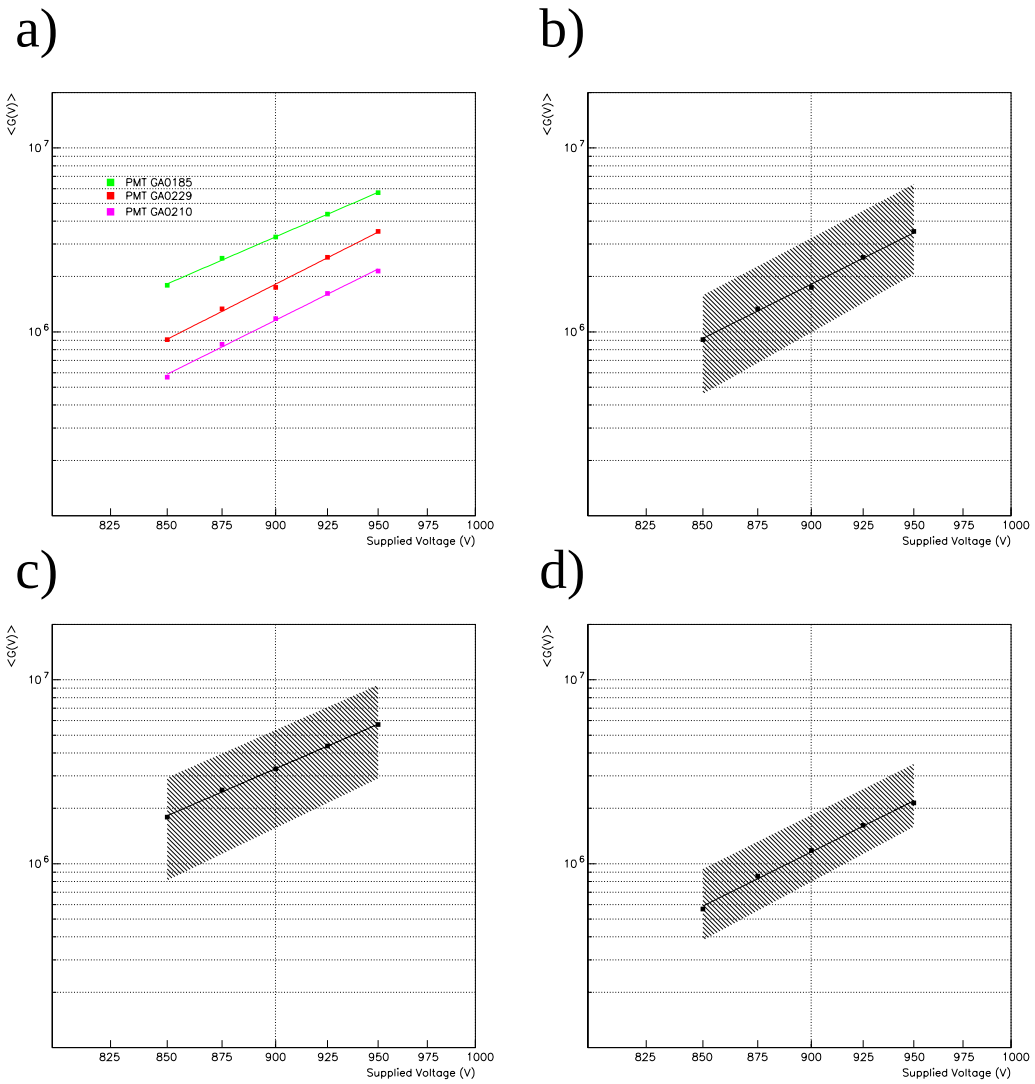

Figure 10. a) Evolution of the mean gain with supplied voltage for PMT GA0229, GA0185, GA0210. The limits of the hatch area correspond to the minimum and maximum gain for PMT's b) GA0229, c) GA0185, d) GA0210.

The results demonstrate that the gain for border channels are lower than those situated in the central PMT area. This is a common characteristic of the 4 studied PMT's. The information brought by the scanning of the two dynodes reveals that their gains are comparable. This is very important for the threshold setting when working at single photoelectron level. However, this is not the case for PMT GA0036 for which the analysis leads to a significant gain dispersion between left and right dynodes for border channels.

Table 1 presents the mean gain, the two extreme values observed on channels of the same PMT and the maximal dispersion which is expressed for one PMT by the ratio $\frac{G_{max}}{G_{min}}$. These measurements indicate that 2 PMT's have a dispersion higher than the Hamamatsu specification limit of 3.

Table 1. Mean values of gain over the 64 channels at 850 V for 4 PMT's.

PMT	Gain ($.10^6$) (V=850 V)			
	$< G(V) >^{central}$	G_{min}	G_{max}	ratio=$\frac{G_{max}}{G_{min}}$
GA0036	7.98	4.04	11.8	2.92
GA0210	6.01	3.69	9.22	2.50
GA0229	10.06	5.38	18.99	3.53
GA0185	17.01	8.19	27.18	3.32

4.4. Evolution of the gain with voltage.

The gain varies strongly as a power of the supplied voltage, $G(V) = KV^{\alpha}$. The measurements obtained by illuminating at single photoelectron level each channel in its geometrical center, were performed for five high voltage values between 850 V and 950 V. The following 3 PMT's GA0210, GA0185, GA0229 were studied.
For the same PMT, varying the voltage, the shape of the gain distribution over the channels remains nearly the same as illustrated Fig. 16, 17, 18. Quantitative results are obtained by fitting for each channel the expression :

$$ln(G_i(V)) = \alpha_i \, ln(V) + \beta_i \ ,$$

with :

$$\beta_i = ln(K_i) \ .$$

Each channel is characterized by the two parameters α_i and β_i of which the mean value and dispersion can be defined for N=64 channels by :

$$< \alpha >= \frac{1}{N} \sum_{i=1}^{N} \alpha_i \ \ , \ \ \sigma_{<\alpha>} = \frac{\sigma_\alpha}{\sqrt{N}}$$

$$< \beta >= \frac{1}{N} \sum_{i=1}^{N} \beta_i \ \ , \ \ \sigma_{<\beta>} = \frac{\sigma_\beta}{\sqrt{N}},$$

where σ_α and σ_β are the RMS of the α and β distributions shown in Fig. 16, 17, 18. The numerical results are given in table 2 for V expressed in *Volts*.

Table 2. Mean values of the parameters characterizing the evolution of each channel with supplied voltage.

PMT	ln G= β + α ln V	
	$< \alpha >$	$< \beta >$
GA0210	11.79 ± 0.13	-66.68 ± 0.85
GA0229	12.02 ± 0.14	-68.70 ± 0.86
GA0185	10.53 ± 0.06	-56.13 ± 0.44

A second analysis is based on the global behaviour of a PMT. This is an important feature which allows to adjust the supplied voltage between PMT's to match with the required mean gain. Consequently, two other parameters are defined, α_{PMT} and β_{PMT} (or K_{PMT}) :

$$< G(V) >= \frac{1}{N} \sum_{i=1}^{N} G_i(V) = K_{PMT} V^{\alpha_{PMT}}$$

$$ln(< G(V) >) = \alpha_{PMT} \, ln(V) + \beta_{PMT} \ .$$

For each PMT, α_{PMT} and β_{PMT} are determined by a fit. Table 3 gives the extracted values.

Table 3. Values of the parameters from linear adjustment concerning the mean behaviour of the PMT with supplied voltage.

PMT	α_{PMT}	β_{PMT}	K_{PMT} (10^6) $[kV]$
GA0210	11.85	-66.64	4.06
GA0229	12.06	-67.63	6.45
GA0185	10.31	-55.16	9.43

The last parameter K_{PMT} gives the mean gain when 1 kV voltage is supplied.
The results shown in table 2 and 3 reveal an important difference of 57% on gain between PMT GA0185 and GA0210 for the same supplied voltage.

5. Crosstalk.

In this part, the crosstalk of PMT GA0229 and GA0185 has been studied (supplied voltage 850 V). This characteristic is evaluated by the fraction of photoelectrons collected by the neighbours of the channel which is illuminated by the WLS fiber located at its geometrical center. The method used to estimate this weak fraction of photoelectrons is based on a precise knowledge of the pedestal shape. Each signal run is preceded by a pedestal run in order to reduce the influence of noise fluctuations during time. An example charge histogram is shown Fig. 11 for channel #18.

5.1. Analysis method.

The number of events registered N_{total} in the pedestal and signal is 10^5. The pedestal histogram, characterized by the peak position Q_0 and the width σ_0, defines a function $P_0(q)$ which will be fitted into the signal histogram on a charge interval [0,Q_{sup}], with $Q_{sup} = Q_0 + 4\sigma_0$.
This scale operation gives a constant which allows to calculate the pedestal part in the signal :

$$P(q) = AP_0(q) \ \ , \ \ \text{A : scale factor} \ ,$$

and the mean number of photoelectrons for neighbouring channels :

$$\begin{aligned} < n_{pe} > \ &= \ -log[\tfrac{N_{pedestal}}{N_{total}}] \\ &= \ -log[\tfrac{\int_0^{+\infty} P(q)dq}{N_{total}}] \\ &= \ -log[A]. \end{aligned}$$

The mean number of photoelectrons on central channel is evaluated using the method exposed in §2.2.
For each channel j, the crosstalk C_j is defined by the

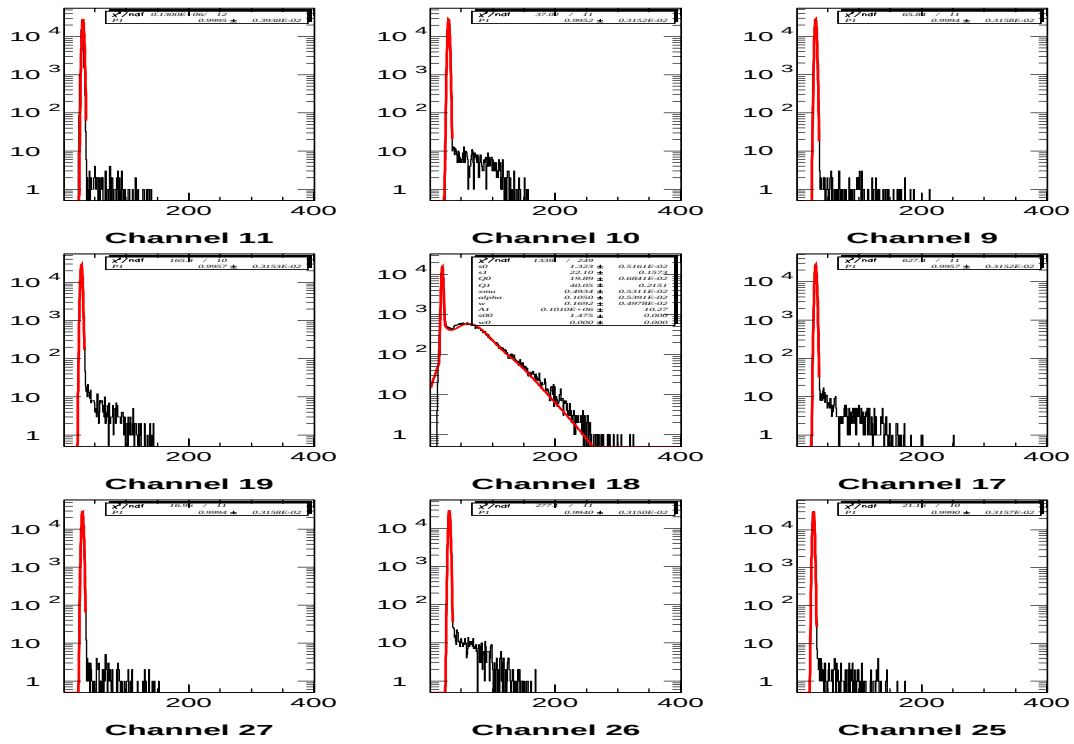

Figure 11. Example of charge histograms obtained on neighbours when the fiber is located on channel #18 for PMT GA0229 (850 V).

ratio of the number of collected photoelectrons by this channel over the total, when the fiber is located on channel i :

$$C_j = \frac{< n_{pe} >_j}{< n_{pe} >_{total}}$$

$$< n_{pe} >_{total} = < n_{pe} >_i + \sum_{j}^{Neighbours\ of\ i} < n_{pe} >_j$$

The sum over all contributions defines the total crosstalk C_i :

$$C_i = \sum_{j}^{Neighbours\ of\ i} C_j \ .$$

5.2. Results and interpretation.

The measurements are summarized by Fig. 19 and 20 for the 2 PMT's.
In each figure, 4 distributions are represented:

- total crosstalk,
- maximum contribution to the crosstalk brought by a neighbouring channel,
- mean value of crosstalk over the four direct neighbouring channels,
- mean value of crosstalk over the diagonal neighbouring channels.

The two first distributions give the total and the maximum fraction of photoelectrons collected by the neighbours for all the 64 channels. The last two allow to compare the repartition of the crosstalk over the neighbouring channels and to quantitatively evaluate the importance of their contribution.
According to this results summarized in Table 4, the maximum contribution for PMT GA0229 is below the limit given by the producer (2%) but for PMT GA0185 it is higher. However, for the 2 PMT's the mean value over the four direct channels are comparable and below the limit for most of the channels. For PMT GA0185 scanning, the fiber was suspected not being at the center of each channel. In order to quantify this shift, the crosstalk asymmetry can be calculated between top-bottom and left-right neighbours :

$$A_{top/bottom} = \frac{C_{top} - C_{bottom}}{C_{top} + C_{bottom}}$$

$$A_{left/right} = \frac{C_{left} - C_{right}}{C_{left} + C_{right}} \ .$$

PMT	Total Crosstalk		Max. Contribution		Mean Crosstalk			
					Side		Corner	
	Mean	RMS	Mean	RMS	Mean	RMS	Mean	RMS
GA0229	5.44 %	1.04 %	1.71 %	0.32 %	1.35 %	0.32 %	0.25 %	0.08 %
GA0185	6.66 %	1.12 %	2.58 %	0.32 %	1.66 %	0.32 %	0.29 %	0.08 %

Table 4. Crosstalk for PMT's GA0229 and GA0185 at 850 V.

PMT	Asymmetry			
	Left/Right		Top/Bottom	
	Mean	RMS	Mean	RMS
GA0229	-0.04	0.11	-0.13	0.08
GA0185	0.54	0.07	0.40	0.06

Table 5. Crosstalk asymmetry for PMT's GA0229 and GA0185 at 850 V.

These variables are expected to be zero when the fiber is well positionned in front of each channel. Their distributions are shown Fig. 21. Border channels which could introduce a bias have been excluded. The results shown in Table 5 confirm that the fiber was not exactly positionned at the center of the channels. This shift is more important for PMT GA0185 and could explain why the maximum contribution is higher than 2%. The mean crosstalk value is less affected by a positionning problem. This misalignment was probably produced after the exact PMT position was determined.

6. Conclusion.

In this article, results concerning gain and crosstalk have been presented for H7546 multianode PMT's. A precise channel scanning has revealed a gain variation inside one channel and a collection efficiency loss of 6% at the center of the channels. This loss is probably due to electrons hitting the focalisation electrode located between the two dynodes. The global scanning has shown that border channels have lower gain than other channels. Consequently, this gives an important dispersion between channels, higher than 3 for two of the four studied PMT's.
Measurements concerning crosstalk have demonstrated that the maximum contribution to the crosstalk remains below 2% for almost all the PMT channels when the WLS fiber is close to the center of each channel.
The next steps in the analysis will be to study the evolution of crosstalk with light intensity.

References

[1] E.H. Bellamy and al., NIM A 339 (1994) 468-476.
[2] Photomultiplier tube, principle to application, HAMAMATSU, 1994.
[3] MINUIT Minimization and error analysis, CERN Geneva, 1999.
[4] NEMO 3 Proposal LAL 94-29 (1994).
[5] OPERA proposal,"*An appearance experiment to search for $\nu_\mu \leftrightarrow \nu_\tau$ oscillations in the CNGS beam*", CERN/SPSC 2000–028, SPSC/P318, LNGS P25/2000, July 10, 2000.
[6] R. Arnold, E. Baussan, M. Dracos, B. Dorion, J–P. Engel, J–L. Guyonnet,J. Cailleret, E. Gamelin, G. Gaudiot, B. Humbert, R. Igersheim,T–D. Le, D. Staub, D. Thomas, J. Wurtz
Plastic Scintillator Target Tracker Proposal, OPERA note #26.
[7] CASCADE User's Guide, CERN ECP/FEX-CA 97-1, Revision 3_01, Mars 1997.
[8] Hamamatsu Photonics K.K., Electron Tube Center, 314–5, Shimokanzo, Toyooka–village, Iwata–gun, Shizuoka–ken, 438–0193, Japan.

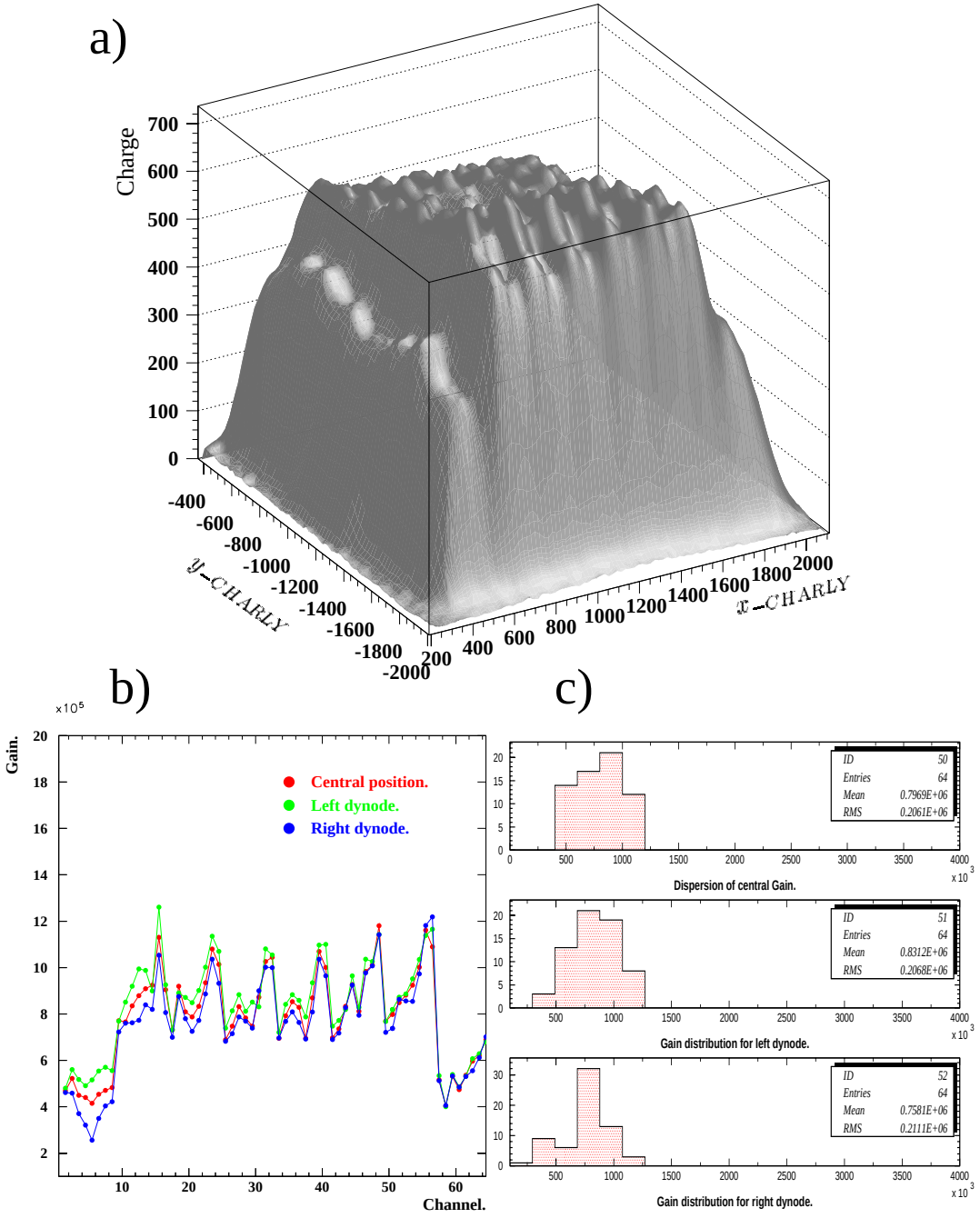

Figure 12. Gain distribution for the PMT GA0036 at 850 V.

a) Charge collection as function of the fiber position (1 scanning step = 20 CHARLY steps = 0.25 mm).
b) Gain of each channel for the WLS fiber in front of the two dynodes and at the center of each channel.
c) Gain distribution for all the channels.

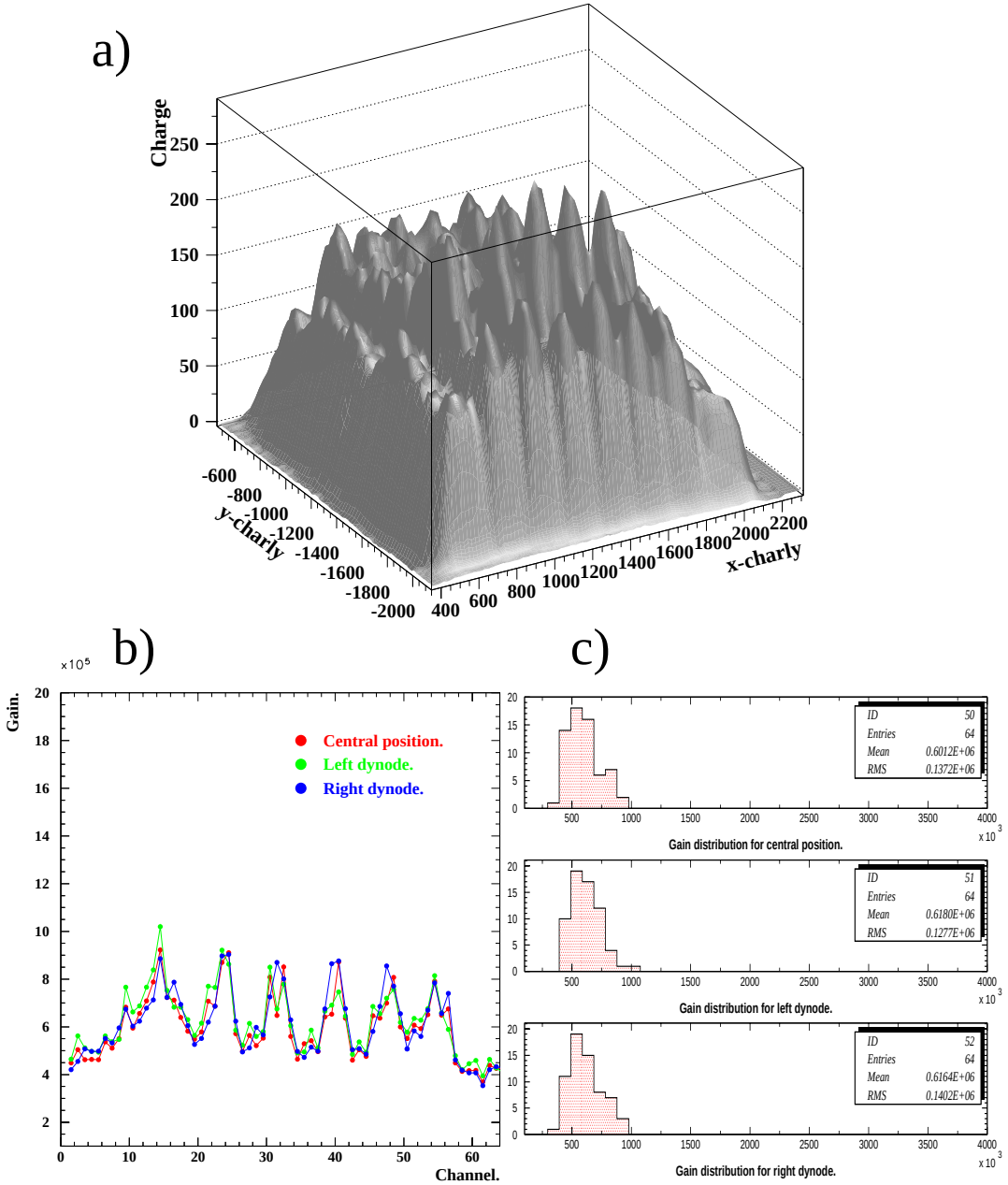

Figure 13. Gain and dispersion by channel for the PMT GA0210 at 850 V.

a) Charge collection as function of the fiber position (1 scanning step = 20 CHARLY steps = 0.25 mm).
b) Gain of each channel for the WLS fiber in front of the two dynodes and at the center of each channel.
c) Gain distribution for all the channels.

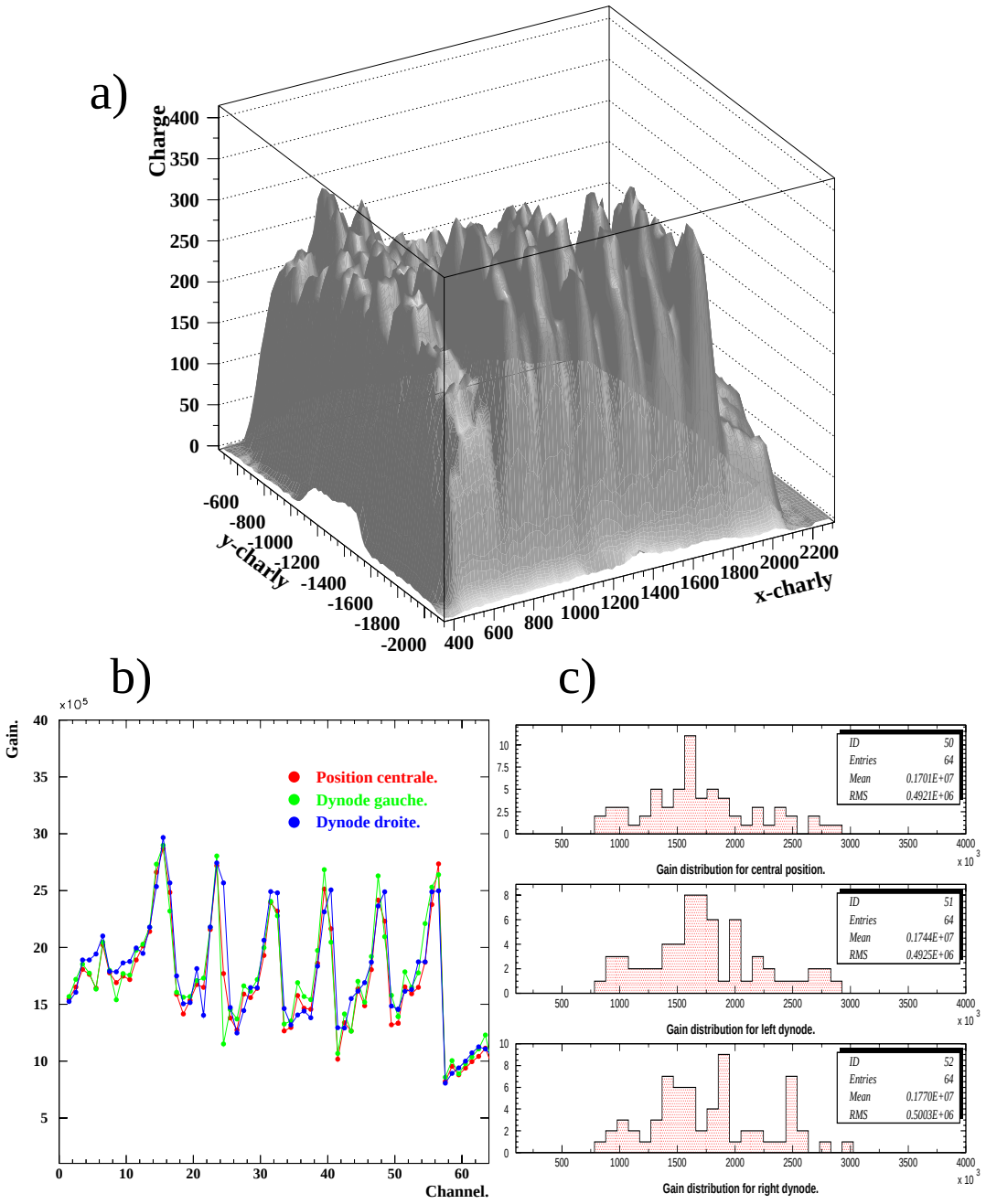

Figure 14. Gain and dispersion by channel for the PMT GA0185 at 850 V.

a) Charge collection as function of the fiber position (1 scanning step = 20 CHARLY steps = 0.25 mm).
b) Gain of each channel for the WLS fiber in front of the two dynodes and at the center of each channel.
c) Gain distribution for all the channels.

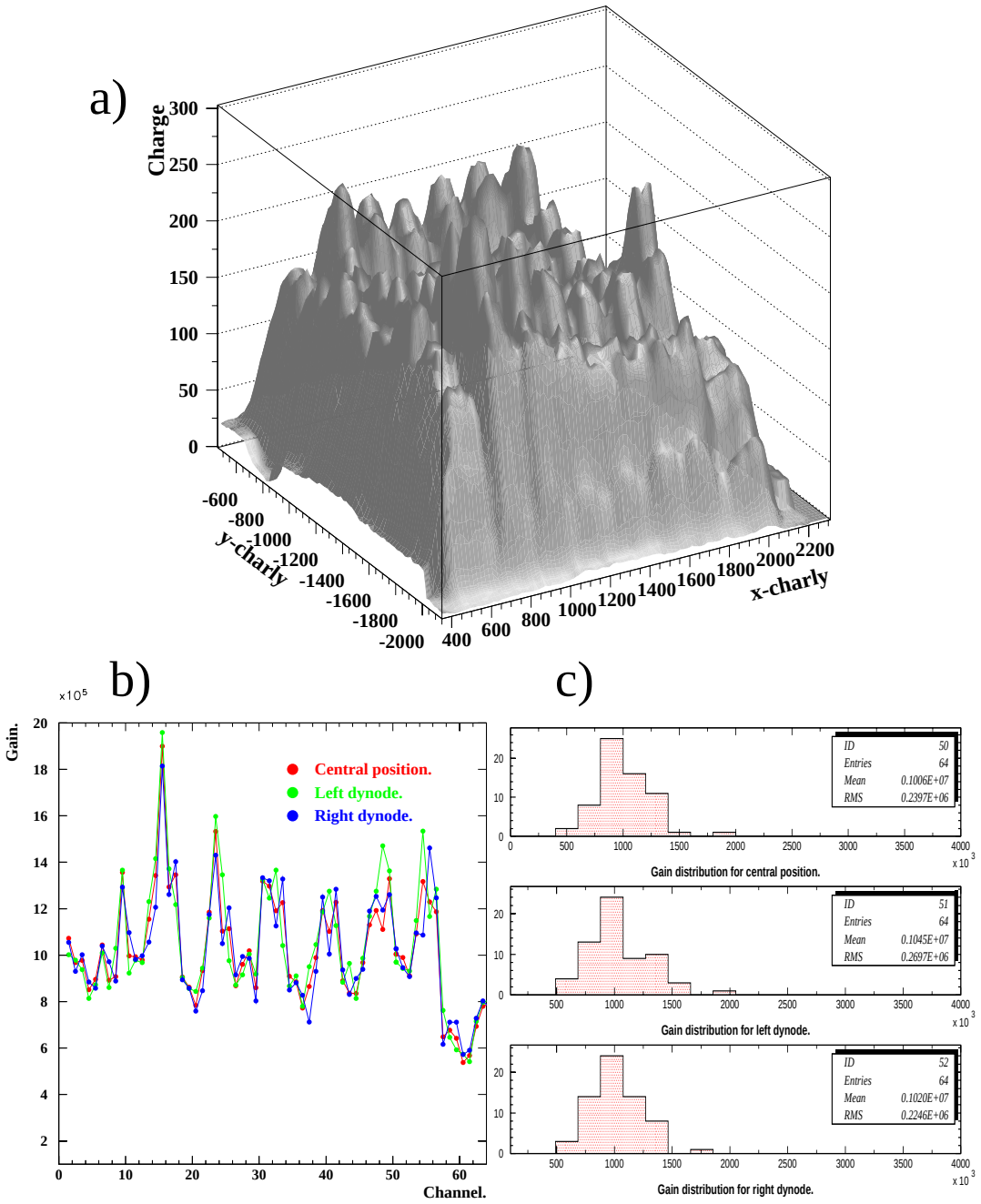

Figure 15. Gain and dispersion by channel for the PMT GA0229 at 850 V.

a) Charge collection as function of the fiber position (1 scanning step = 20 CHARLY steps = 0.25 mm).
b) Gain of each channel for the WLS fiber in front of the two dynodes and at the center of each channel.
c) Gain distribution for all the channels.

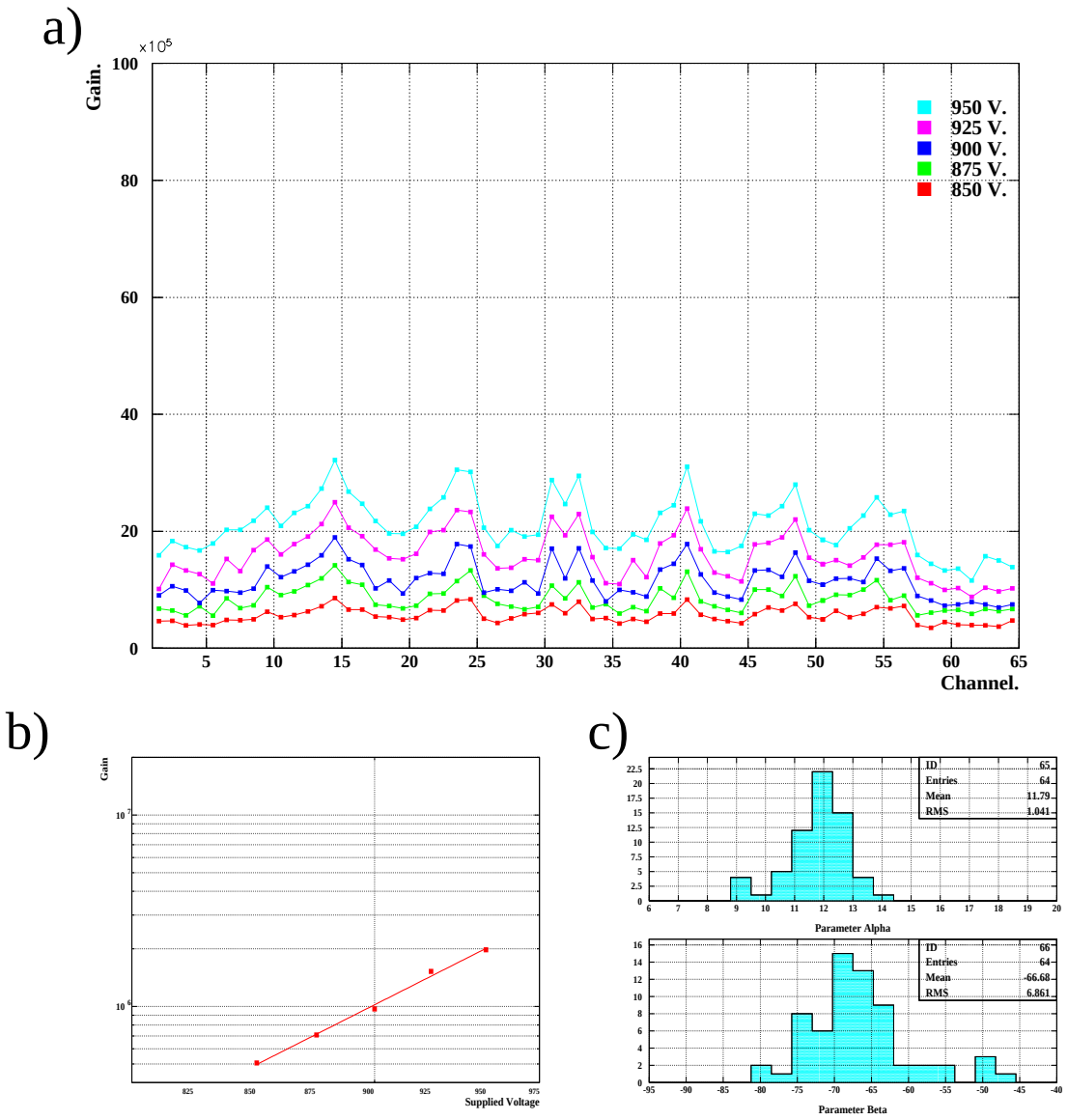

Figure 16. Gain variation for the PMT GA00210.

a) Gain per channel for different high voltage values.
b) Gain variation for channel #36.
c) α and β parameter distribution.

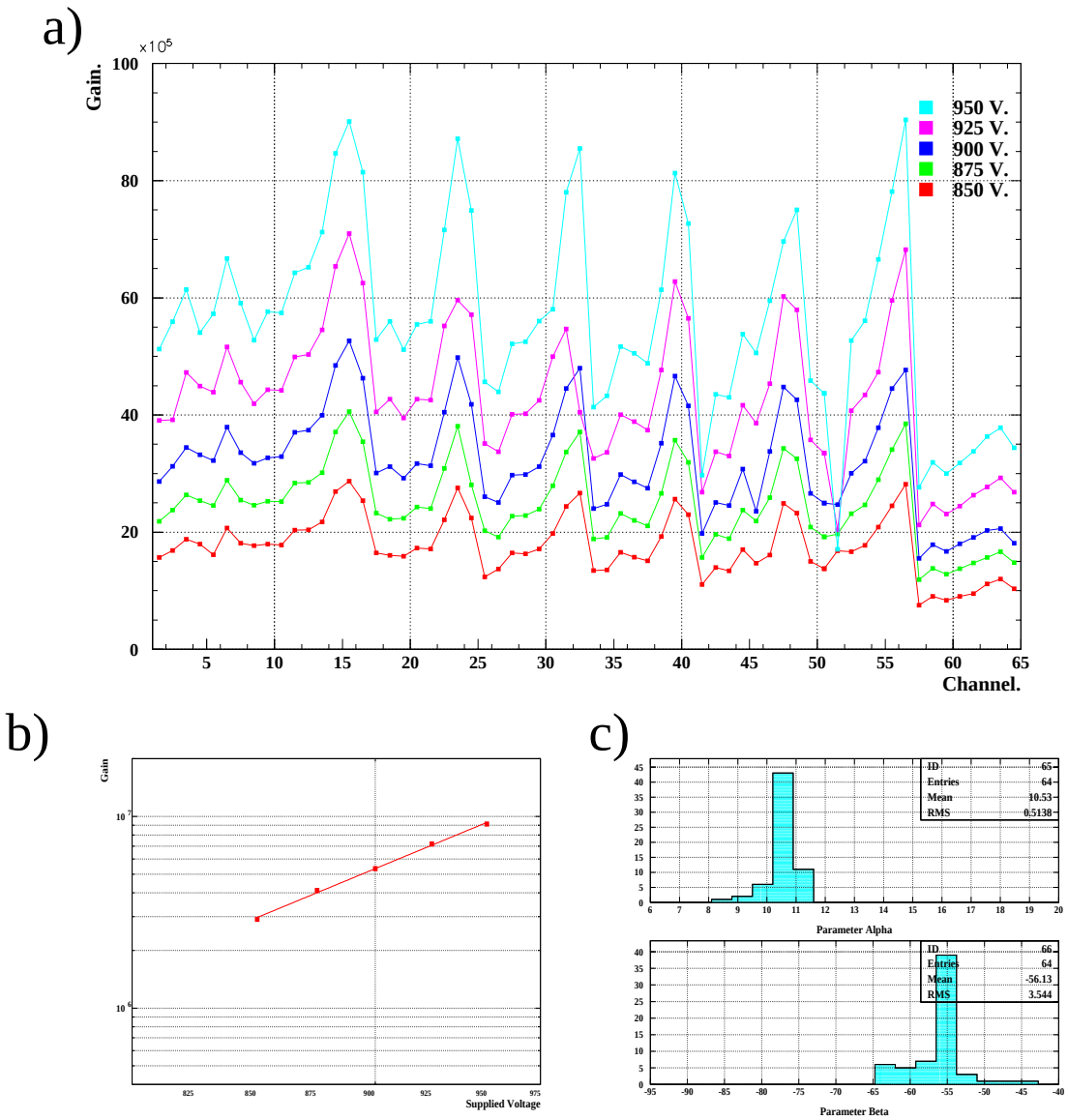

Figure 17. Gain variation for the PMT GA0185.

a) Gain per channel for different high voltage values.
b) Gain variation for channel #15.
c) α and β parameter distribution.

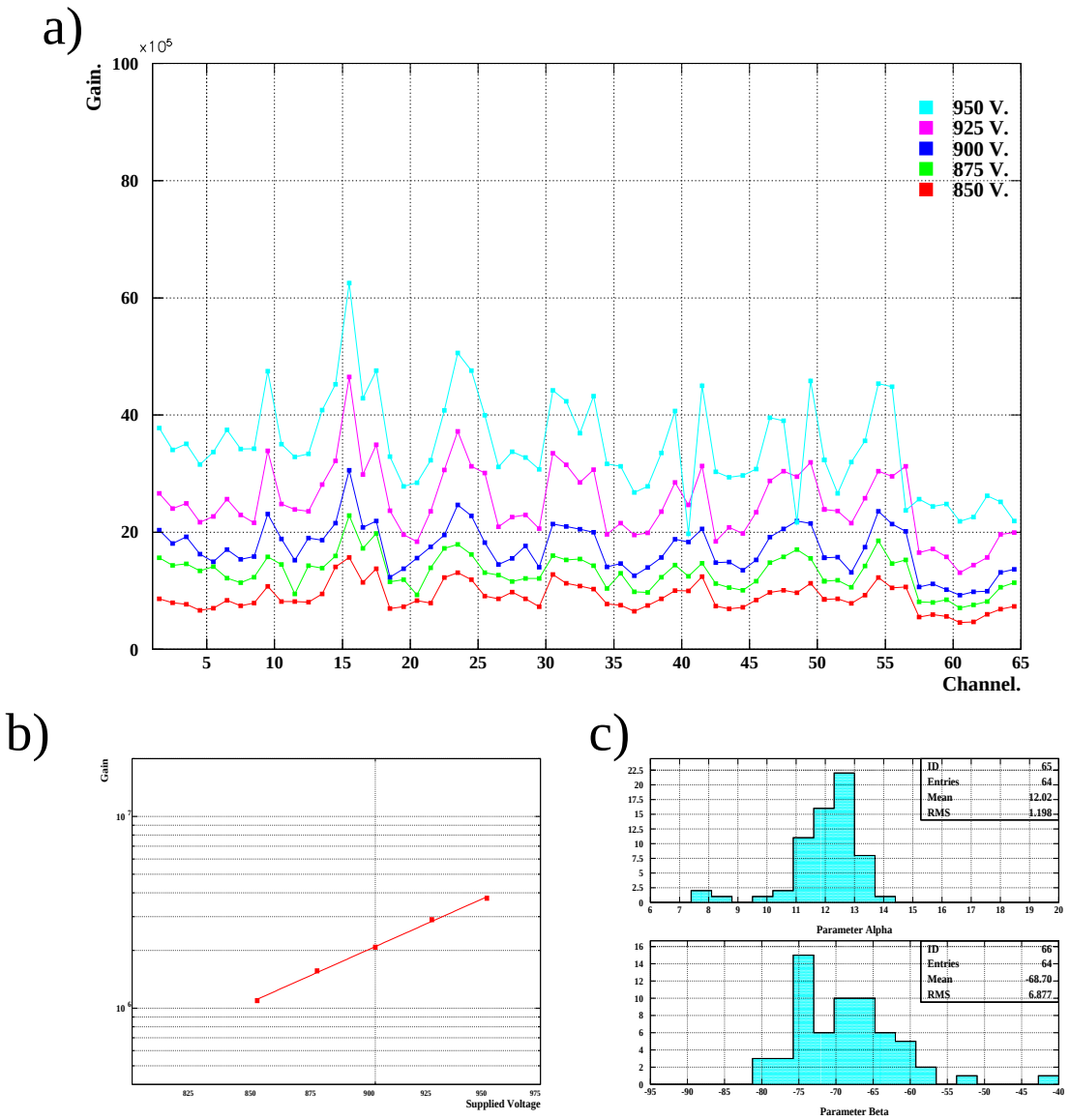

Figure 18. Gain variation for the PMT GA0229.

a) Gain per channel for different high voltage values.
b) Gain variation for channel #32.
c) α and β parameter distribution.

a)

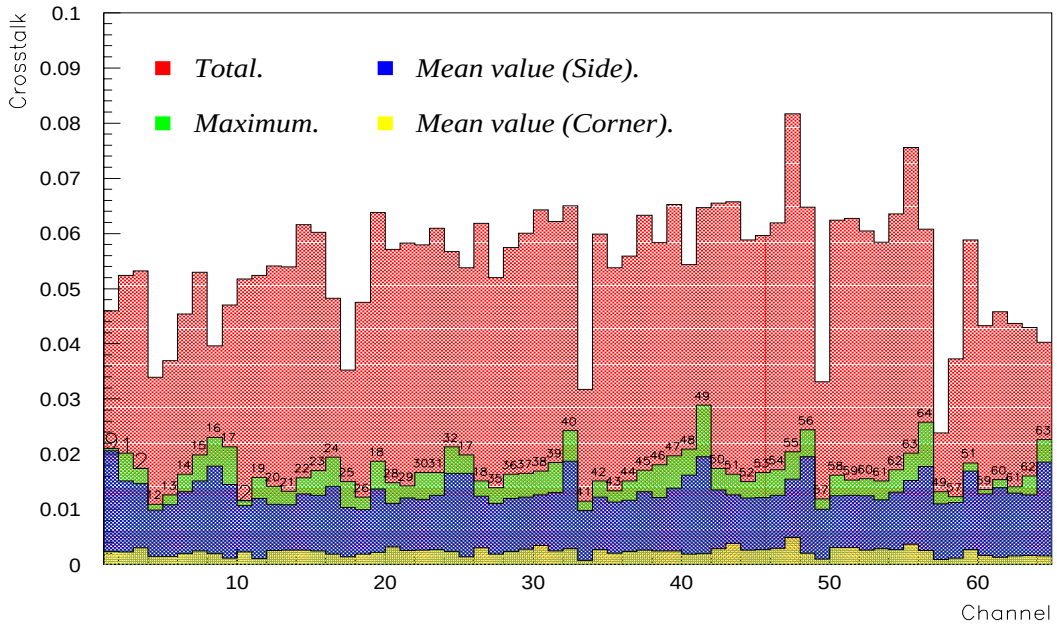

b)

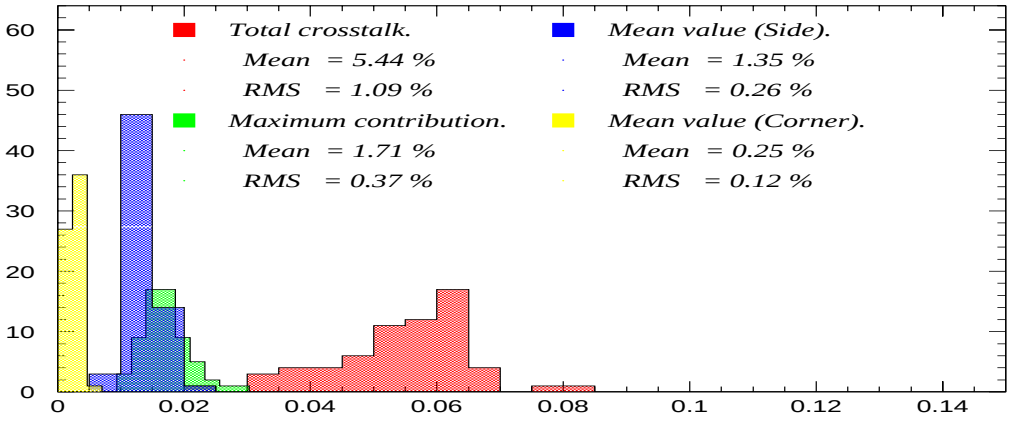

Figure 19. Crosstalk of PMT GA0229 at 850 V.

a) Crosstalk per channel : total crosstalk (on all neighbouring channels), maximum crosstalk contribution by one neigbouring channel of which its number is indicated above each bin, mean crosstalk on direct neighbours and corner neighbourgs.
b) Corresponding crosstalk distributions.

a)

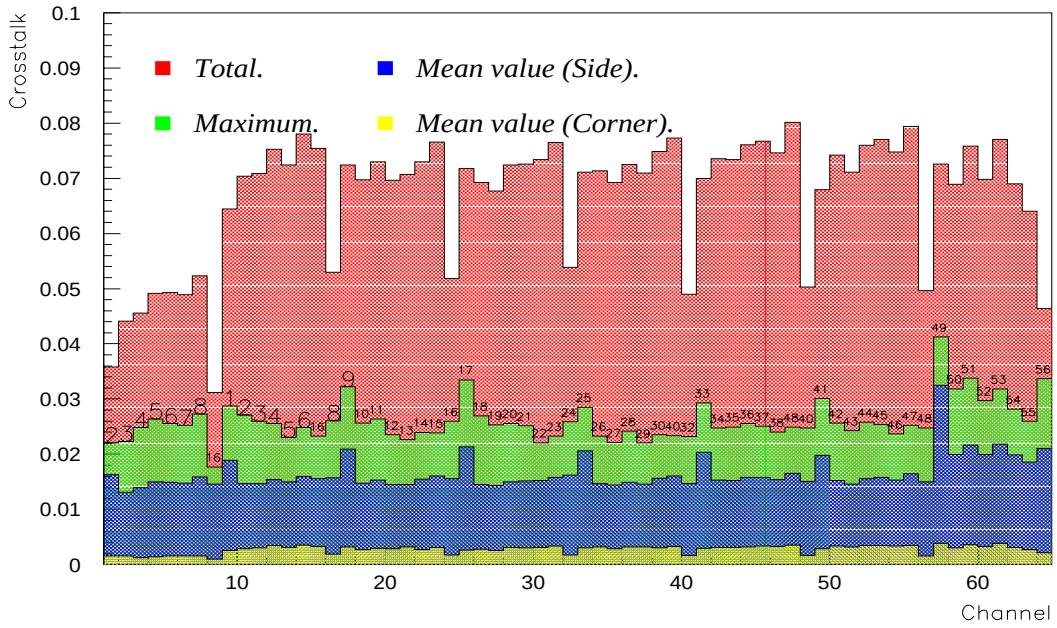

b)

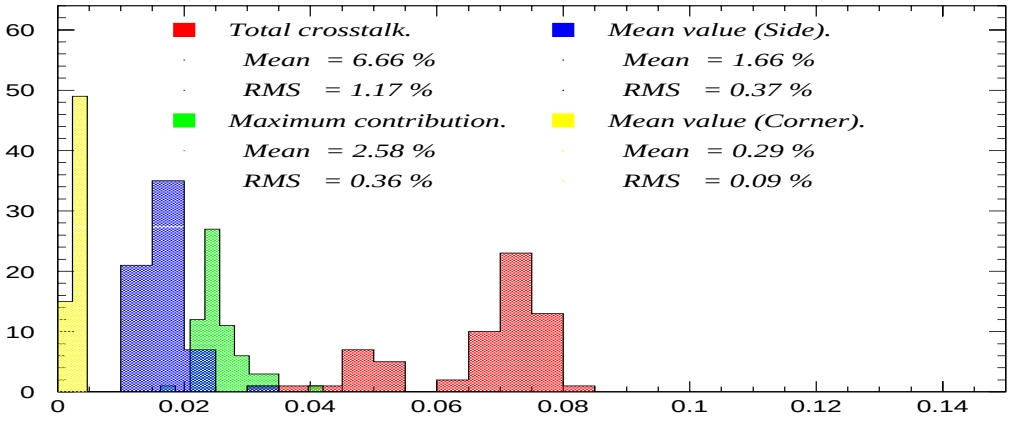

Figure 20. Crosstalk of PMT GA0185 at 850 V.

a) Crosstalk per channel : total crosstalk (on all neighbouring channels), maximum crosstalk contribution by one neigbouring channel of which its number is indicated above each bin, mean crosstalk on direct neighbours and corner neighbourgs.
b) Corresponding crosstalk distributions.

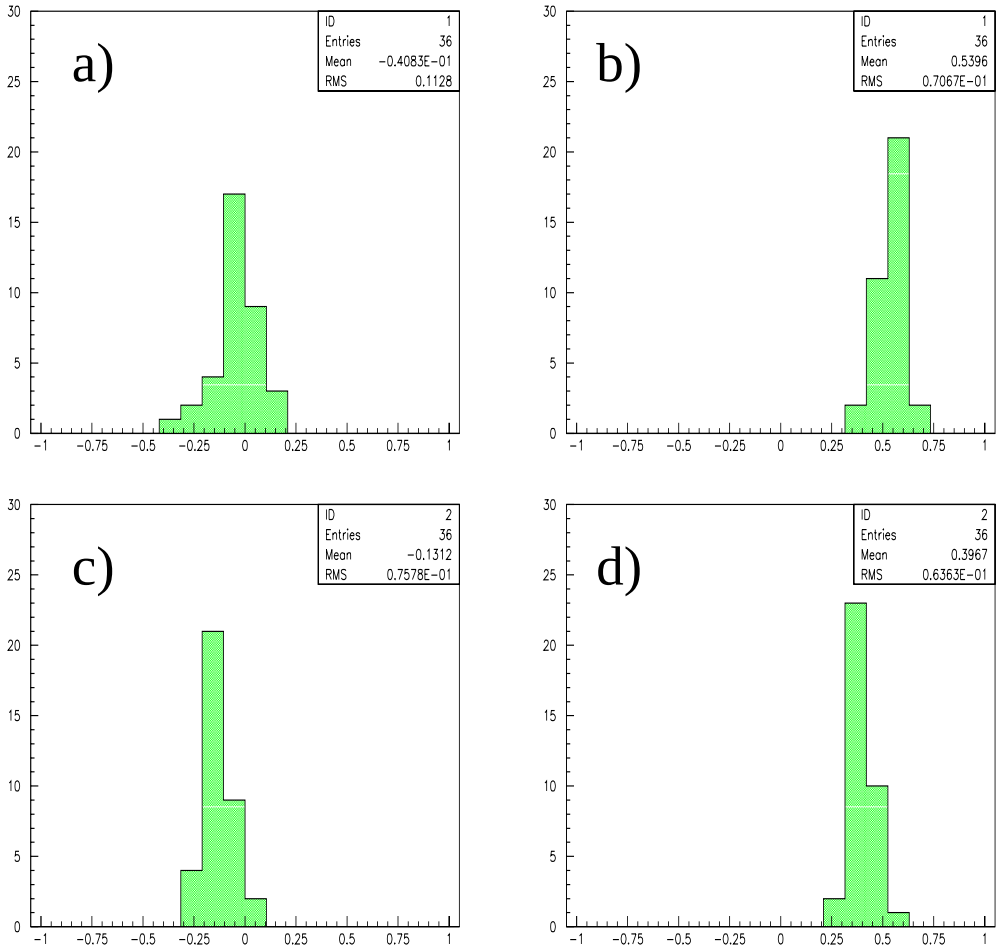

Figure 21. Crosstalk asymmetry distributions.

Left/right asymmetry a) GA0229, b) GA0185.
Top/bottom asymmetry c) GA0229, d) GA0185.